Thermodynamic Tetragonal Phase Stability in Sol−Gel Derived Nanodomains of Pure Zirconia

Satyajit Shukla and Sudipta Seal*

Advanced Materials Processing and Analysis Center (AMPAC), and Mechanical Materials Aerospace Engineering (MMAE) Department, Engineering # 381, 4000 Central Florida Blvd., University of Central Florida, Orlando, Florida 32816

Received: November 19, 2003; In Final Form: January 26, 2004

Nanocrystalline (15−30 nm) and submicron-sized (500−600 nm) zirconia (ZrO_2) particles are synthesized using the sol−gel technique. The metastable tetragonal phase is stabilized at room temperature within pure ZrO_2 nanodomains of size 15−45 nm having nonspherical morphology. Using thermodynamic analysis, it is revealed that the critical nanosize for tetragonal phase stabilization, at room temperature, may vary depending on the contribution from the surface, interfacial, and strain energies, which determine the size and the shape of the tetragonal nanodomains.

Introduction

Zirconia (ZrO_2) primarily exists in three different polymorphs at ambient pressure: monoclinic (room temperature-1175 °C), tetragonal (1175−2370 °C), and cubic (2370−2680 °C). The room-temperature monoclinic phase has no practical applications since its formation during cooling from the high-temperature tetragonal phase is associated with the volume expansion, which results in crumbling of the ceramic components. On the other hand, the high-temperature ZrO_2 phases are suitable for various industrial applications such as solid electrolytes in solid oxide fuel cells[1] and sensors,[2] as a catalyst/catalyst support,[3,4] and as membranes[5] and dispersed phase in composite materials.[6] Hence, traditionally high-temperature ZrO_2 phases have been stabilized at room temperature by doping trivalent cations in the ZrO_2 lattice.[7]

The high-temperature tetragonal phase can also be stabilized at room temperature without doping any trivalent impurities, provided ZrO_2 is synthesized in its nanocrystalline form with size less than a critical nanosize.[8] Thus, above and below this critical nanosize, monoclinic and tetragonal phases exist, respectively. There are contradictory reports in the literature,[9,10] which show the stability of the tetragonal phase above the critical nanosize and that of the monoclinic phase below it. Since these reports synthesize nanocrystalline ZrO_2 under different conditions, it appears that the critical nanosize for the tetragonal phase stabilization in nanocrystalline ZrO_2 is not a constant but may change under specific conditions, which in turn affects the stability range of the involved phases. The involvement of several factors such as surface energy, interfacial energy, and strain-energy may affect the critical nanosize for the tetragonal phase stabilization at room temperature. As a result, the high-temperature tetragonal phase may be stabilized, at room temperature, in the nanodomains of different sizes having different morphologies (spherical as well as nonspherical). The experimental results reported in the literature, in support of this hypothesis, are rather scattered. Moreover, the current understanding of the observed phenomenon also appears to be incoherent. From this point of view, the main objectives of the present letter are set to demonstrate the stabilization of the tetragonal phase at room temperature within pure ZrO_2 nanodomains of size greater than the critical nanosize reported earlier,[8] and to justify this effect on the basis of the variation in the critical nanosize for the tetragonal phase stabilization, which is determined using thermodynamic and strain energy considerations.

* Corresponding author. Phone: (407) 823-5277, Fax: (407) 823-0208, e-mail: sseal@pegasus.cc.ucf.edu

Experimental Section

Zirconium(IV) *n*-propoxide, anhydrous ethanol (200 proof), and the HPC polymer (molecular weight: 80 000−370 000 g/mol) are obtained from Aldrich chemicals and are used as received.

Nanocrystalline ZrO_2 powder is synthesized in the present investigation via hydrolysis of zirconium(IV) *n*-propoxide in an alcohol solution. The beakers used in the experiments were cleaned, washed with deionized water, dried completely, and rinsed with anhydrous 200 proof ethanol before use. During synthesis, two different but equal parts of alcohol solutions were prepared. In the first part, deionized water was dissolved into anhydrous ethanol in a specific proportion. An appropriate amount of HPC polymer, with selected molecular weight, was then added and dissolved completely by stirring the solution overnight using a magnetic stirrer. The second part of the alcohol solution was then prepared by completely dissolving a specific amount of zirconium(IV) *n*-propoxide (this amount was kept constant for all experiments involved in this investigation) in anhydrous ethanol under atmospheric conditions. The solution was homogenized using magnetic stirring for 1−2 minutes only. After preparing each solution, both the beakers were sealed immediately with paraffin tape. Hydrolysis of zirconium(IV) *n*-propoxide was then carried out under atmospheric conditions by rapidly mixing the two sealed solutions under vigorous stirring. The formation of ZrO_2 particles, due to immediate precipitation, was evident from the white color of the resulting sol. The sol was stirred very slowly for 4 h and then held under static conditions for 24 h to ensure completion of the hydrolysis and condensation reactions. The sol was subsequently dried at 80 °C using Petri dishes in order to remove the solvent

10.1021/jp037532x CCC: $27.50
Published on Web 02/19/2004

completely. The small gel pieces obtained were then crushed to obtain the nanocrystalline ZrO_2 powder.

The nanocrystalline ZrO_2 powder was synthesized using the above method under various processing conditions by varying the ratio of molar concentrations of water and zirconium(IV) *n*-propoxide (R), the concentration ([HPC]), and the molecular weight (MW_{HPC}) of the HPC polymer. The concentration of zirconium(IV) *n*-propoxide was kept constant for all experiments (0.1 M). The R-value, [HPC], and MW_{HPC} were respectively varied within the range of 5−60, 1.0−2.0 g/L, 80 000−370 000 g/mol. The synthesis conditions utilized in this investigation are such that 100% tetragonal phase is obtained after calcining the as-synthesized amorphous ZrO_2 powder at 400 °C. The as-synthesized nanosized ZrO_2 powders were subjected to the calcination treatment within the temperatures ranging from 300 to 1000 °C in air for the phase evolution study. The samples were heated at a rate of 30 °C/min up to the calcination temperature, held at that temperature for 2 h, and then furnace cooled to room temperature.

The crystalline phases present in the calcined powders were determined using a standard Rigaku X-ray diffractometer (XRD). Line traces were obtained over 2θ values ranging from 10°−80°. Narrow scan analysis was conducted in the 2θ range of 27°−32° as it contained the strongest line for the tetragonal $(111)_T$ phase. This intense peak was then curve-fitted using the peak-fit software (peak-fit, version-4, SPSS Inc.). The average tetragonal crystallite (or nanodomain) size (D_T) was calculated from the $(111)_T$ diffraction peaks using Scherrer equation[11] as shown below,

$$D_T = (0.9\lambda)/(\beta \cos\theta) \quad (1)$$

where D_T is the average tetragonal nanocrystallite (nanodomain) size in nm, λ the radiation wavelength (0.154 nm), β the corrected half-width at half-maximum intensity (fwhm), and θ the diffraction peak angle.

The as-synthesized and calcined ZrO_2 powders were further examined using scanning electron microscope (SEM) and transmission electron microscope (TEM) to obtain the particle size distribution within the submicron sized and the nanosized ZrO_2 powders, respectively.

Results

A SEM image of submicron sized ZrO_2 particles synthesized under the processing conditions R = 5, [HPC] = 1.0 g/L, MW_{HPC} = 80 000 g/L is presented in Figure 1a. Monodispersed, spherical ZrO_2 particles of size 500−600 nm are synthesized under these processing conditions. A TEM image of nanosized ZrO_2 particles, synthesized under the processing conditions of R = 30, [HPC] = 2.0 g/L, MW_{HPC} = 80 000 g/L is shown in Figure 1b. Agglomerated, faceted (nonspherical) ZrO_2 nanoparticles of size 15−30 nm are obtained under these processing conditions, forming aggregates of size 70−80 nm. Few porous, large sized ZrO_2 nanoparticles are also visible in Figure 1b. The as-synthesized ZrO_2 powders, Figure 1, are X-ray amorphous. However, they crystallized into 100% tetragonal structure after calcination at 400 °C for 2 h. Only the nanosized ZrO_2 powder synthesized under the processing conditions R = 60, [HPC] = 2.0 g/L, MW_{HPC} = 80 000 g/L, exhibited partial tetragonal crystallization at lower calcination temperature (300 °C).

A typical broad-scan XRD pattern obtained after crystallization of submicron-sized ZrO_2 powder, synthesized under the processing conditions R = 5, [HPC] = 1.0 g/L, MW_{HPC} = 80 000 g/L, is presented in Figure 2, where the major $(111)_T$ peak of tetragonal ZrO_2 is identified. All other peaks in the XRD pattern also belong to the tetragonal crystal structure. The submicron-sized ZrO_2 powder thus essentially crystallizes into tetragonal crystal structure with strong $(111)_T$ orientation after the calcination treatment. A SAED pattern, obtained from the center of one of the spherical, submicron-sized particles, after the crystallization, is shown as an inset in Figure 3. A large

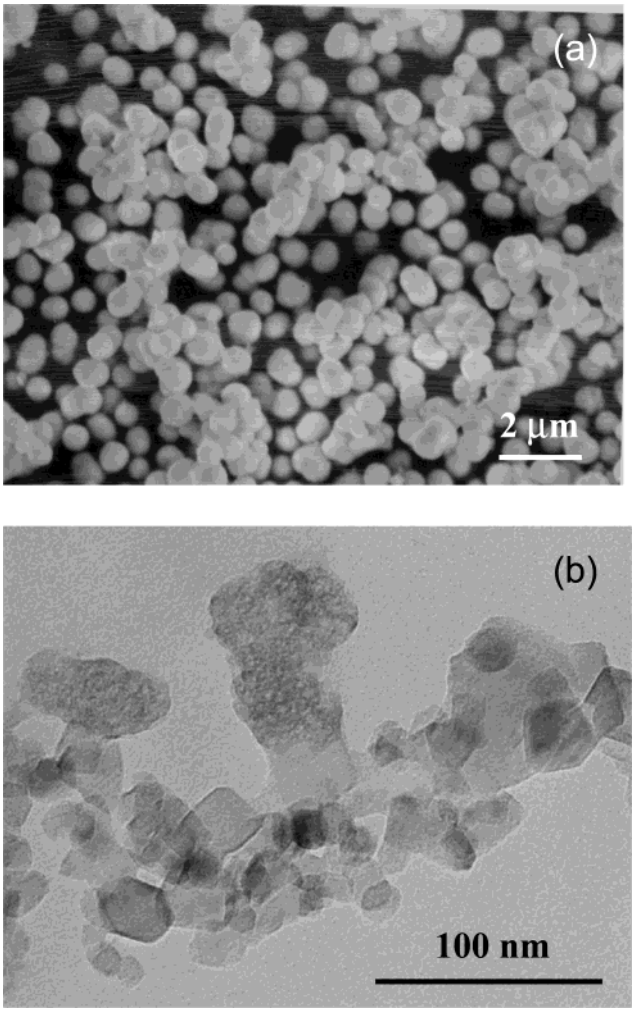

Figure 1. SEM (a) and TEM (b) images of sol−gel derived ZrO_2 particles synthesized under the processing conditions of R = 5, [HPC] = 1.0 g/L and R = 30, [HPC] = 2.0 g/L. MW_{HPC} = 80 000 g/mol.

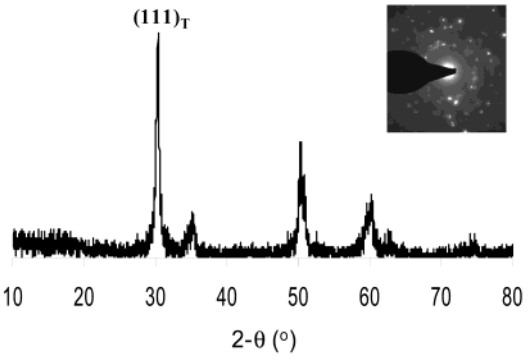

Figure 2. Typical room-temperature broad-scan XRD patterns obtained for monodispersed, spherical, submicron-sized ZrO_2 particles after crystallization at 400 °C. R = 5, [HPC] = 1.0 g/L, MW_{HPC} = 80 000 g/mol. (inset) SAED pattern obtained from the center of one of the spherical particles.

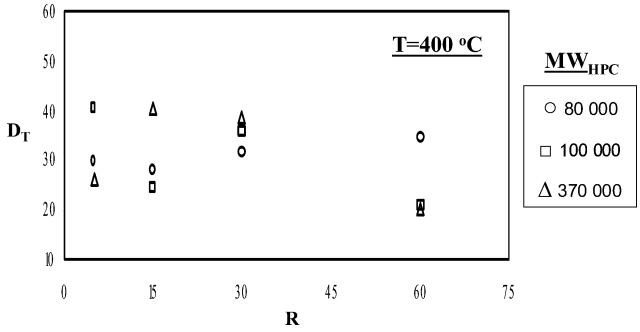

Figure 3. Variation in the tetragonal nanodomain size as a function of *R*, observed for the sol−gel derived nanocrystalline ZrO_2, synthesized using the HPC polymer having different molecular weights. For MW_{HPC} = 80 000 g/mol, [HPC] = 2.0 g/L and for MW_{HPC} = 100 000 g/mol and 370 000 g/mol, [HPC] = 1.0 g/L.

number of diffraction spots are observed in the SAED pattern, which further confirms the crystalline nature of the spherical particles after the crystallization at 400 °C. From the SAED pattern it is also inferred that the submicron sized, spherical ZrO_2 particles, after the crystallization, are composed of a large number of nanocrystallites having different orientations. Using the full width at half-maximum intensity (fwhm) of the $(111)_T$ peak, Figure 2, obtained via narrow scan analysis, the average tetragonal nanodomain size of 45 nm is calculated. Hence, the spherical, monodispersed ZrO_2 particles of size 500−600 nm are composed of tetragonal nanodomains of 45 nm size after the crystallization at 400 °C.

The variation in the tetragonal nanodomain size (determined using eq 1) as a function of *R*, after the crystallization at 400 °C, obtained for the nanocrystalline ZrO_2 synthesized using the HPC polymer having various molecular weights, is presented in Figure 3. The synthesis conditions in Figure 3 are such that either submicron-sized or nanocrystalline-aggregated ZrO_2 particles with 100% tetragonal phase are obtained after the calcination treatment at 400 °C. In Figure 3, the tetragonal nanodomain size is observed to decrease marginally with increasing *R*-value within the range of 5−60. The overall tetragonal nanodomain size is observed to be within the range of 20−40 nm. Thus, the maximum tetragonal nanodomain size of 40 nm is detected after the calcination treatment at 400 °C.

The variation in the average tetragonal nanodomain size as a function of the calcination temperature, obtained for the nanocrystalline ZrO_2 powder synthesized under the processing conditions of [HPC] = 2.0 g/L, MW_{HPC} = 80 000 g/L for different R-values, is shown in Figure 4. The different phases existing at room temperature, after the calcination treatment at higher temperatures, are also marked in Figure 4. It is observed that, at 400 °C, which is the crystallization temperature, 100% tetragonal phase is obtained. Tetragonal-to-monoclinic phase transformation is observed within the calcination temperature range of 600−800 °C, above which 100% monoclinic phase is obtained. It is also noted that, with increasing calcination temperature, the average tetragonal nanodomain size increases (except for *R* = 60, where small decrease is observed at lower calcination temperatures). The average tetragonal nanodomain size reaches a maximum value of 40 nm, under all processing conditions, before 100% monoclinic phase is detected. It appears that 40 nm is a critical nanosize for stabilizing the tetragonal structure under the given processing conditions. Moreover, this critical nanosize of 40 nm, determined using the calcination treatment, is identical with the stabilization of the tetragonal structure within the maximum nanodomain size of 40 nm at the crystallization temperature of 400 °C, Figure 3.

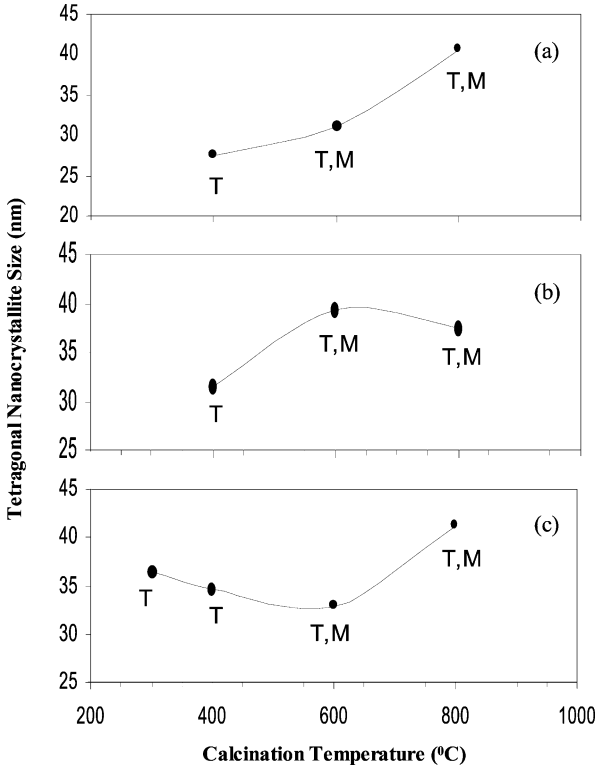

Figure 4. Variation in the tetragonal nanodomain size as a function of calcination temperature, observed for the sol−gel derived nanocrystalline ZrO_2, synthesized under the processing conditions: [HPC] = 2.0 g/L, MW_{HPC} = 80 000 g/mol. (a) *R* = 15, (b) *R* = 30, (c) *R* = 60.

Discussion

In the present investigation, nanocrystalline and submicron-sized nonspherical and spherical ZrO_2 particles containing 100% tetragonal phase are synthesized by crystallizing the sol−gel-derived amorphous ZrO_2 powders (synthesized under different processing conditions) at 400 °C. It is observed that the tetragonal phase is stabilized within the nanodomains of different sizes depending on the processing conditions. In Figure 1a, the tetragonal phase is stabilized within nonspherical nanodomains of average size 45 nm (determined using XRD) within spherical submicron-sized (500−600 nm) ZrO_2 particles. Moreover, the tetragonal phase is stabilized within aggregated and faceted (nonspherical) ZrO_2 nanoparticles of size 15−30 nm, Figure 1b, after the calcination treatment. Moreover, the maximum average tetragonal nanodomain size of 40 nm is observed after crystallization, Figure 3, which is identical with the maximum tetragonal nanodomain size observed during the calcination treatment, Figure 4. It is thus noted that the high-temperature tetragonal phase of ZrO_2 is stabilized at room temperature, within the nanodomains of size 15−45 nm.

It is well known that a strain-free, pristine (newly prepared single crystal with no prior thermal history) bulk monoclinic ZrO_2 single-crystal transforms into a tetragonal structure at 1175 °C at ambient pressure. The monoclinic-to-tetragonal phase transformation temperature, however, decreases with decreasing particle size.[12] As a result, there exists a critical nanoparticle size below which the high-temperature tetragonal phase can be stabilized at room temperature. Thermodynamic consideration shows that,[13,14] for a strain-free, isolated ZrO_2 nanocrystal, the critical nanosize (D_c) for the monoclinic-to-tetragonal phase transformation, at room temperature, is given by the relationship

$$D_c = -6(\sigma_t - \sigma_m)/q\,(1-T/T_b) \qquad (2)$$

where σ_t and σ_m are the surface free energies (J/m^2) of the tetragonal and monoclinic phases respectively, q the heat of transformation, T and T_b the transformation temperatures for nano and bulk single crystals, respectively. Substituting[8,13,14] $\sigma_t = 0.77$ J/m^2, $\sigma_m = 1.13$ J/m^2, $q = 2.82 \times 10^{+8}$ J/m^3, $T =$ 300 K, and $T_b = 1448$ K, the critical nanosize for the monoclinic-to-tetragonal phase transformation, at room temperature, is calculated to be 10 nm. Thus, the tetragonal structure, which provides lower surface energy gets stabilized below 10 nm critical nanosize. Analogous to a liquid droplet on the solid surface, which tends to attain a spherical surface morphology by minimizing its surface energy, a single, isolated, strain-free ZrO_2 nanocrystal of size less than 10 nm must possess a spherical (or near-spherical) surface morphology since the surface energy difference overcomes the volume free energy difference of the involved phases, below this critical nanosize. High-resolution TEM (HRTEM) images of single, isolated, strain-free, tetragonal ZrO_2 nanocrystals with a spherical (or near-spherical) surface morphology, as reported by Chraska et al.[14] and Nitsche et al.,[15] support this hypothesis. Moreover, the change in the shape of the particle from the initial spherical shape to spindle- or rod-like shape due to the tetragonal-to-monoclinic phase transformation has also been reported by Noh et al.[16]

It is, however, noted that the ZrO_2 nanoparticles, synthesized under the specific conditions, are not single, isolated particles but form aggregates, Figure 1b. As a result, the surface energies of the ZrO_2 nanoparticles are modified. Moreover, during the calcination treatment, the average ZrO_2 nanoparticle size within the aggregates increases, Figure 4, which suggests the existence of coherency between the ZrO_2 nanocrystallites within the aggregates. Hence, if we assume that the tetragonal ZrO_2 nanoparticles within the aggregates are similar to the coherent precipitates and tend to transform into noncoherent monoclinic particles, then the modified surface energy (interfacial energy) values, σ_t and σ_m, can be taken as 0.22 J/m^2 and 1.46 J/m^2 for coherent-tetragonal and noncoherent-monoclinic nanocrystallites, respectively.[13] Substituting these modified surface energy (interfacial energy) values in eq 2, the critical nanosize of 33 nm is calculated for the tetragonal phase stabilization within an aggregate. It appears that the critical nanosize increases from 10 to 33 nm when the single, isolated ZrO_2 nanocrystals become elements of an aggregated particle. Hence, the critical nanosize for the tetragonal-to-monoclinic phase transformation is larger when the ZrO_2 nanocrystals form aggregates than that when they exist as isolated, single, spherical (or near-spherical) nanocrystals. In the present investigation, ZrO_2 nanoparticles of size 15−30 nm, forming aggregates in the as-synthesized condition, crystallize into tetragonal structure (and do not transform into monoclinic structure) after the calcination treatment at 400 °C since their size is below the critical nanosize of 33 nm required for the tetragonal-to-monoclinic phase transformation in an aggregated condition.

The tetragonal nanodomains within an aggregate may undergo grain growth during the calcination treatment, as demonstrated in Figure 4. Hence, when the size of the tetragonal nanodomains increases beyond 33 nm, the tetragonal structure should be transformed into monoclinic structure. However, we detect maximum tetragonal nanodomain size of 40 nm during the calcination treatment. The tetragonal-to-monoclinic phase transformation is known to be associated with 5% volume expansion. As a result, if the surrounding aggregate matrix is sufficiently rigid to prevent this transformation, the transforming tetragonal nanodomain within an aggregate may be subjected to the hydrostatic stresses. Second, if the surrounding matrix also tends expand due to the tetragonal-to-monoclinic phase transformation, then the tetragonal nanodomain under consideration may be subjected to the additional hydrostatic stresses. The hydrostatic stresses (or strains) produced via these two mechanisms would be stored in the tetragonal nanodomains in the form of lattice defects such as dislocations and ionic defects.[9] In the presence of hydrostatic strain energy stored within the tetragonal nanodomains, the critical nanosize is given by[9,13]

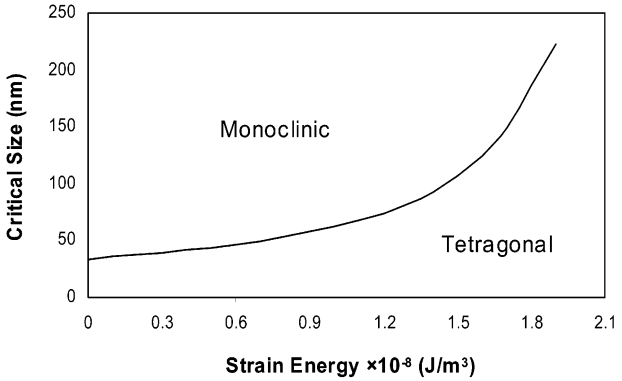

Figure 5. Variation in the critical nanosize as a function of hydrostatic strain energy calculated using eq 3.

$$D_c = -6(\sigma_t - \sigma_m)/[q(1-T/T_b) + \Delta\epsilon_{m\rightarrow t}] \qquad (3)$$

where, $\Delta\epsilon_{m\rightarrow t}$ is the hydrostatic strain-energy difference between the tetragonal and monoclinic phases. Garvie[13] estimated a strain-energy difference of -0.46×10^8 J/m^3 arising from the misfit of the tetragonal particles in the cubic matrix. Hence, substituting $\Delta\epsilon_{m\rightarrow t} = -0.46 \times 10^8$ J/m^3 and the modified surface energy (interfacial energy) values in eq 3, a new critical nanosize for the tetragonal-to-monoclinic phase transformation is calculated to be 41 nm. The stabilization of the tetragonal phase within the nanodomains of size 40 nm, Figures 3 and 4, is in excellent agreement with the calculated critical nanodomain size of 41 nm. Hence, it appears that, in the present investigation, the stabilization of the tetragonal phase within the nanodomains of size 40 nm, observed in the present investigation, involves significant contribution from the strain energy along with that of the modified surface energy (interfacial energy).

The variation in the critical nanosize as a function of hydrostatic strain energy, obtained using eq 3, is presented in Figure 5. As mentioned earlier, the critical nanosize for the tetragonal phase stabilization in a strain-free, isolated single crystal is 10 nm, where the lower surface energy is solely responsible for the tetragonal phase stabilization. The critical nanosize increases to 33 nm as a result of modification in the surface energy (interfacial energy) due to an aggregation of strain-free ZrO_2 nanoparticles. As demonstrated in Figure 5, the critical nanosize increases well above 33 nm with increasing amount of hydrostatic strain-energy stored within the tetragonal nanodomains. This satisfactorily explains the stabilization of the tetragonal nanodomains of size 45 nm within the monodispersed, spherical, submicron-sized (500−600 nm) ZrO_2 particles and also within the nanodomains as large as 100 nm reported by others.[9]

It is concluded that the surface energy, the interfacial energy (modified surface energy), and the strain energy are the three

major factors that determine the critical nanosize for the high-temperature tetragonal phase stabilization at room temperature within the sol−gel derived nanodomains of ZrO_2. For a strain-free, isolated, single ZrO_2 nanocrystal of size less than 10 nm, the surface energy difference balances the volume free energy difference of the particle, thus stabilizing the tetragonal phase in a spherical nanoparticle. For the size range of 10−33 nm, the interfacial energy (modified surface energy) difference balances the volume free energy difference of the particles, thus stabilizing tetragonal phase in nonspherical (faceted) and aggregated nanoparticles. For the size range above 33 nm, the volume free energy is balanced by the strain energy and the interfacial energy (modified surface energy) differences, thus stabilizing the tetragonal phase in nonspherical, strongly aggregated nanoparticles.

Acknowledgment. The authors take this opportunity to thank National Science Foundation EEC 0136710, 0085639 for financial support. Authors are also thankful to the Materials Characterization Facility (MCF) at the University of Central Florida (UCF).

References and Notes

(1) Drennan, J. *J. Mater. Synth. Process*. **1998**, *6*, 181−189.
(2) Haefele, E.; Kaltenmaier, K.; Schoenauer, U. *Sens. Actuators B* **1991**, *4*, 525−527.
(3) Yamaguchi, T. *Catal. Today* **1994**, *20*, 199−218.
(4) Turlier, P.; Dalmon, J. A.; Martin, G. A.; Vergnon, P. *Appl. Catal.* **1987**, *29*, 305−310.
(5) Pavlik, R. S., Jr.; Klein, L. C.; McCauley, R. A. *J. Am. Ceram. Soc.* **1995**, *78*, 221−224.
(6) Porter, D. L.; Evans, A. G.; Heuer, A. H. *Acta Metallogr*. **1979**, *27*, 1649−1654.
(7) Li, P.; Chen, I.-W.; Penner-Hanhn, J. E. *J. Am. Ceram. Soc.* **1994**, *77*, 1281−1288.
(8) Garvie, R. C. *J. Phys. Chem.* **1965**, *69*, 1238−1243.
(9) Mitsuhashi, T.; Ichiara, M.; Tatsuke, V. *J. Am. Ceram. Soc*. **1974**, *57*, 97−101.
(10) Morgan, P. E. D. *J. Am. Ceram. Soc.* **1984**, *67*, C-204−C-205.
(11) Cullity, B. D. *Elements of X-ray Diffraction*; Addison-Wesley: Reading, MA, 1978.
(12) Garvie, R. C.; Goss, M. F. *J. Mater. Sci.* **1986**, *21*, 1253−1257.
(13) Garvie, R. C. *J. Am. Ceram. Soc.* **1978**, *82*, 218−224.
(14) Chraska, T.; King A. H.; Berndt, C. C. *Mater. Sci. Eng. A* **2000**, *286*, 169−178.
(15) Nitsche, R.; Winterer, M.; Hahn, H. *Nanostruct. Mater*. **1995**, *6*, 679−682.
(16) Noh, H.-J.; Seo, D.-S.; Kim, H.; Lee, J. K *Mater. Lett.* **2003**, *57*, 2425−2431.